Analysis of the 2008 Markarian 421 Flare with VERITAS

By Casey Allard

Advised by Dr. Jodi Christiansen

Physics Department

California Polytechnic State University

San Luis Obispo, California

Table of Contents

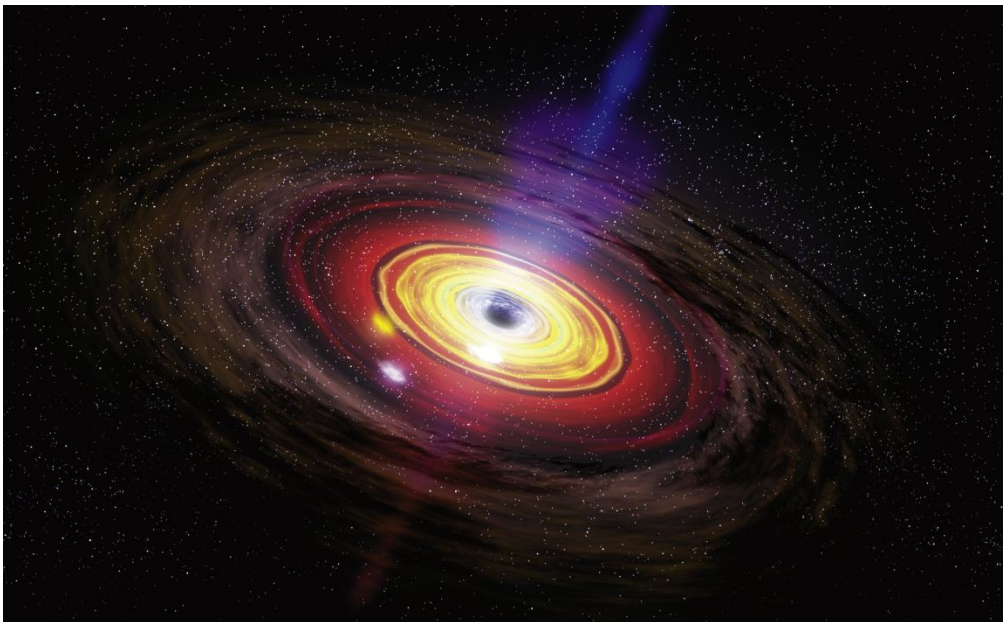

http://www2.le.ac.uk/departments/physics/postgraduate-study/images/Blackhole-1920.jpg

Abstract

A theoretical light curve model is fit to an observed short term flare of Markarian (Mrk) 421 in the very high energy spectrum. The flare is characterized by its measured light curve from the Very Energetic Radiation Imaging telescope Array System (VERITAS). The flare we analyzed occurred in May 2008. We successfully fit a theoretical model to the Mrk 421 data light curve. The data appears to agree with the Wagner [1] and Salvati [2] models. These models appear to fit both broad and sharp flaring regions found in the measured light curve. Furthermore the Wagner model is used to calculate the emission region sizes of the blazar, or the region of the blazar form which the observed gamma rays were emitted. The upper limit to the size of these emission regions is also calculated. The emission regions are found to be equivalent in size to planetary orbits in our solar system. This is relatively small for a region of a galactic sized object such as a blazar, indicating an unexpected conclusion to the agreeing theoretical models.

I. Introduction

The vastness of our universe is too great for the human eye to observe all of its wonder. There are members of our universe, whole galaxies, which are too far away for their intricacies to be seen even by our best telescopes. One unique galactic sized phenomenon in our universe that is very far away is the blazar. A blazar is a type of intergalactic object known as an Active Galactic Nuclei (AGN). AGN reside in the centers of many galaxies, and are known for, among other things, their emission of high energy gamma rays. AGN are interesting because they sometimes brighten or flare significantly. A flare is an increase in flux above the normal steady state flux from an observable source. This means that the amount of gamma rays emitted by an AGN per unit time has increased by a significant amount. Because the distance between AGN and earth is so great, the reasons why these high energy gamma rays are emitted from these mysterious objects is often hypothesized with theoretical models. These models hypothesize the parameters of AGN and the reasons why they emit such high energy photons.

This paper models a measured light curve of the May 2008 flare of Markarian 421 observed with VERITAS. The goal of this project is to find a theoretical model that agrees with the measured light curve, and to analyze the results of the model to make conclusions regarding the specific parameters of the AGN.

II. Theory of Blazars

Active Galactic Nuclei (AGN) are quasi-stellar objects that are believed to contain two relativistic particle jets separated by an accretion disk, which has a black hole at its center. The specification that defines an AGN as a Blazar is that one of the relativistic jets is aimed towards Earth. AGNs with jets that do not point in the direction of Earth are called quasars, Seyfert Galaxies, or radio galaxies. The typical length size of a jet is 100-200 kpc. In comparison, the diameter of our Milky Way galaxy is 30 kpc. The relativistic particle jets are thought to be

generated by a super massive black hole at their origin, which pulls matter from the surrounding accretion disk into two magnetic fields which collimate it into a cone shaped jet.

Like many Blazars, Mrk 421 exhibits rapid variability in its observed light curve. This means that the high energy source flares over very short time periods. This is the main focus of our research on Mrk 421. The Blazar seems to exhibit very irregular short time-period flares. We attempted to determine the size of this irregular flaring by fitting a theoretical model of Mrk 421.

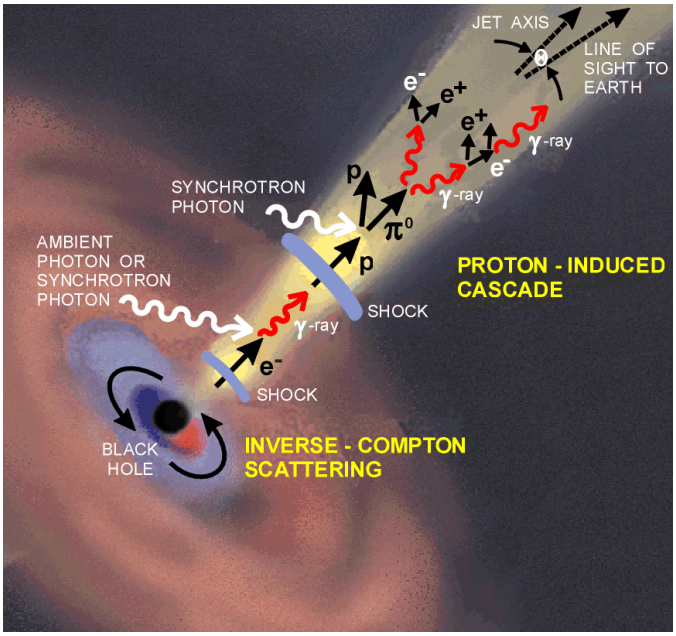

Figure 1: Artist's conception of the particle flow of a jet in Active Galactic Nuclei [3]

There are currently two types of models used to describe high energy flux observations of AGN, leptonic and hadronic models. The main difference between the two models is that leptonic models predict that gamma rays are emitted by inverse Compton scattering, but hadronic models predict that gamma ray emissions are caused by proton decay products in the jet. Figure 1 represents both of these models. The electron interaction originating at the innermost shock front is a representation of the leptonic model, the proton interaction originating from the outer shock front is a depiction of the hadronic model. Notice that Figure 1 shows both models absorbing an ambient or Synchrotron photon. The leptonic model begins with a blob of electrons injected into the jet. When this photon collides with an electron in the jet moving at a relativistic speed, Inverse Compton scattering occurs. Compton scattering is caused by the interaction of a photon with an electron. A photon collides with an electron ionizing it and exciting it to a higher energy. The electron quickly de-excites by emitting a photon with a lower energy than the original photon. Inverse Compton scattering is the process taking place in the leptonic model of figure 1. The difference between Inverse Compton scattering and Compton scattering is that instead of a photon striking a nearly stationary electron, the photon is striking a relativistic electron in the jet of the Blazar. This fast moving electron emits a higher energy photon than the photon that it originally collided with. The fact that synchrotron photons are involved in the inverse Compton scattering process as a part of the leptonic model is the reason that it is sometimes called the Synchrotron-Self Compton model. The hadronic model begins with a blob of protons injected into the jet. When these protons, moving at relativistic speeds, collide with ambient or synchrotron photons in the jet, they create a particle cascade much like the one depicted in figure 1. This proton induced cascade generates high energy gamma rays that travel along the line of sight to Earth, just like the leptonic model. The fact that the two models use particle interactions

as a means of producing high energy gamma rays suggests that the Spectral Energy Distribution (SED) emitted from AGN is non-thermal [1].

This paper analyzes the high energy flaring of Markarian 421 due to either the leptonic or hadronic model. We believe the cause of the flaring to be blobs of accretion disk matter that are transported toward the pole of the black hole and then "injected" into the relativistic particle jets. As a blob of electrons or protons enters the jet it is bombarded by relatively low energy photons which causes the photons to become excited to higher energies due to inverse Compton scattering. This blob bombardment is believed to occur at the narrow region of the jet very close to the black hole. The deterioration of the blob in the jet can be seen in the light curve from VERITAS. As the relativistic jet particles begin colliding with the blob, the light generated from the front part of the blob (the part closest to Earth) reaches telescopes on Earth first. This is described by the equation $d = c\Delta t$ where c is the speed of light in a vacuum. Since the front part of blob is closer to earth than the backside of the blob, it will reach Earth in a shorter amount of time. The beginning of a flare or the upward curve of flux vs. time, on a light curve is seen at the time that the first light generated by the shock front reaches our telescopes. This is known as the rise time and is indicative of the size of the blob in the jet. The rise time is caused by the inverse Compton scattering of the electrons in the blob as discussed previously. After the electrons have undergone inverse Compton scattering they no longer have any energy and therefore cannot emit any more gamma rays. The observable decrease in the flare, form the peak of the flare to its end, is an indication of the number of energized electrons left in the jet over time. This is known as the cooling time. One interesting note about the gamma rays emitted from the jet is that, due to the relativistic speeds of particles in the jet, all of the emitted gamma rays from the jet pointed toward earth are perceived to be emitted toward Earth. I say perceived because in the particle rest frame gamma rays are emitted in all directions, but the relativistic curvature of space time directs more of the gamma rays toward Earth in the observers frame.

III. Theory of Flaring

The blazar emission models discussed are concerned more with rapid flares rather than long term flares of the AGN. What is a "rapid" flare? Every model that I use in this paper to describe rapid variability of Markarian 421 fits mathematical theories to flares that begin and end within one night of observation. For this work we will take a "rapid" flare to mean a flare that lasts less than one full night of observations, or approximately 7 hours.

To generate a model of the 2008 flare of Markarian 421, we explored two different theoretical models. The models discuss relatively longer and shorter, more rapid flares, allowing a highly adjustable model capable of satisfying all needed conditions. Wagner et. al. [1] gives the flux flaring function:

$$F(t) = F_{SS} + a_0 * (2^{\frac{t-t_0}{\tau_{fall}}} + 2^{\frac{-(t-t_0)}{\tau_{rise}}})^{-1} \qquad (1)$$

as a description for sub hour flaring of Markarian 421. This function, though time dependent, is primarily dependant on four parameters. F_{SS} is the Steady state flux associated with any observation. a_0 is the flare amplitude, which is defined as the difference in flux, associated with Markarian 421 in its flaring state vs. its non-flaring state. τ_{rise} and τ_{fall} are the exponential rise and fall times of the flare. This function is simplified when used to describe one flare per night, but it can be useful in describing pile-up flares [1]. The variability of theses flares can be traced back to the region of the jet from which they were emitted. The parts of the jet closest to the central black hole of the AGN have the highest amount of energy. A diagram of the jet with different energy regions is shown in Figure 2 [4]. The energy difference is indicated by the decrease in frequency of emitted photons from the jet farther from the central black hole. This decrease in energy and emission frequency is caused by the collisions of particles in the jet with ambient or synchrotron photons. When a blob of electrons or photons is injected into the jet, and undergoes an energy exchange reaction such as inverse Compton scattering, the resulting particle has much less energy than it began with. The first reaction results in the emission of high energy gamma rays from the jet. Afterwards, the lower energy particles which have already undergone a reaction can be struck with more ambient photons causing them to react again. These later reactions with lower energy electrons and photons farther down the jet result in the emission of lower energy photons from the source.

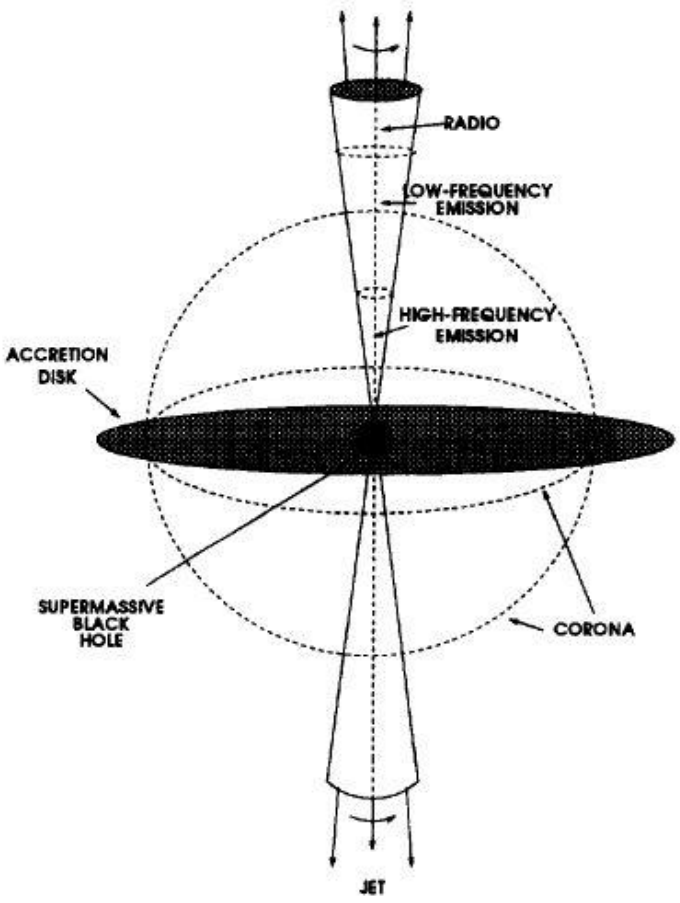

Figure 2: Geometric model of an AGN. This model includes the regions of the jet which emit photons at different energy values [4].

For this reason, the physical particles of the jet are thought to move the fastest when they are closest to the black hole. The telescopes that observed Markarian 421 which the data was collected from observed the blazar emissions form only the region of the jet identified as "High-Frequency Emission" in Figure 2. We can use the Doppler boosting factor (δ), which is only relevant in this region, and the time scale over which the source variability occurs to determine what part of the high-frequency emission region of the blazer jet the gamma rays were emitted

from. The very high energy gamma rays, 50 GeV to 50 TeV energy range, are hypothesized to be generated form a small emission region of the jet near the super massive black hole. The observation of photon emissions this close to the origin of the jet can give us clues about the physics of the injection mechanisms of AGN [2]. The Doppler boosting factor is describe by the equation

$$\delta = \frac{1}{1+z} * \frac{1}{\Gamma(1-\beta\cos(\theta))} \qquad (2)$$

It is called the Doppler boosting factor because it accounts for the Doppler shifting of light as seen by observers on Earth. The Doppler boosting factor has two main parts. The first part of the equation contains the red shift of the source, z. Not only does this describe the distance of the source from the observer, it also identifies the length contraction of the source as seen by the observer. The second part of the equation is known as the beaming factor. The beaming factor describes the geometry of the relativistic jet, where Γ is the Lorentz factor, β is the bulk jet motion speed $\beta = (1-\frac{1}{\Gamma^2})^{\frac{1}{2}}$, and θ is the jet viewing angle. The beaming factor accounts for the curvature of space-time due to the superluminal motion of the jet.

The upper limit for the radius of the emission region is given by

$$R < c2\tau_{\text{rise}}\delta \qquad (3)$$

This is the region of the relativistic particle jet from which the observed high energy gamma rays are emitted. Equation 3 shows that the size of the emission region is heavily dependent on both the Doppler boosting factor δ and the rise time of the flare. A flare with a smaller rise time indicates gamma rays emitted from a region of the jet closer to the central super massive black hole, or the origin of the jet. A smaller flare rise time also indicates a smaller blob injected into the jet, where smaller is a description of the physical size or number of particles contained in blob. Therefore, a smaller blob is associated with a smaller light emission region as expected.

Another mathematical description of these rapid flares is described in [2]. The coordinates of shock fronts in the jet and the flux created by them over time are shown in Figure 3.The x coordinate is given by

$$x = \frac{c}{\sin(\theta)}[t_{obs} - t(1-\beta\cos(\theta)] \qquad (4)$$

Where c is the speed of light in a vacuum, θ is the observers line of sight through the jet, t_{obs} is the observers time, t is the time, and $\beta = (1-\frac{1}{\Gamma^2})^{\frac{1}{2}}$.

On a cone, the y coordinate is given by:

$$y = \sqrt{s^2 - x^2} \qquad (5)$$

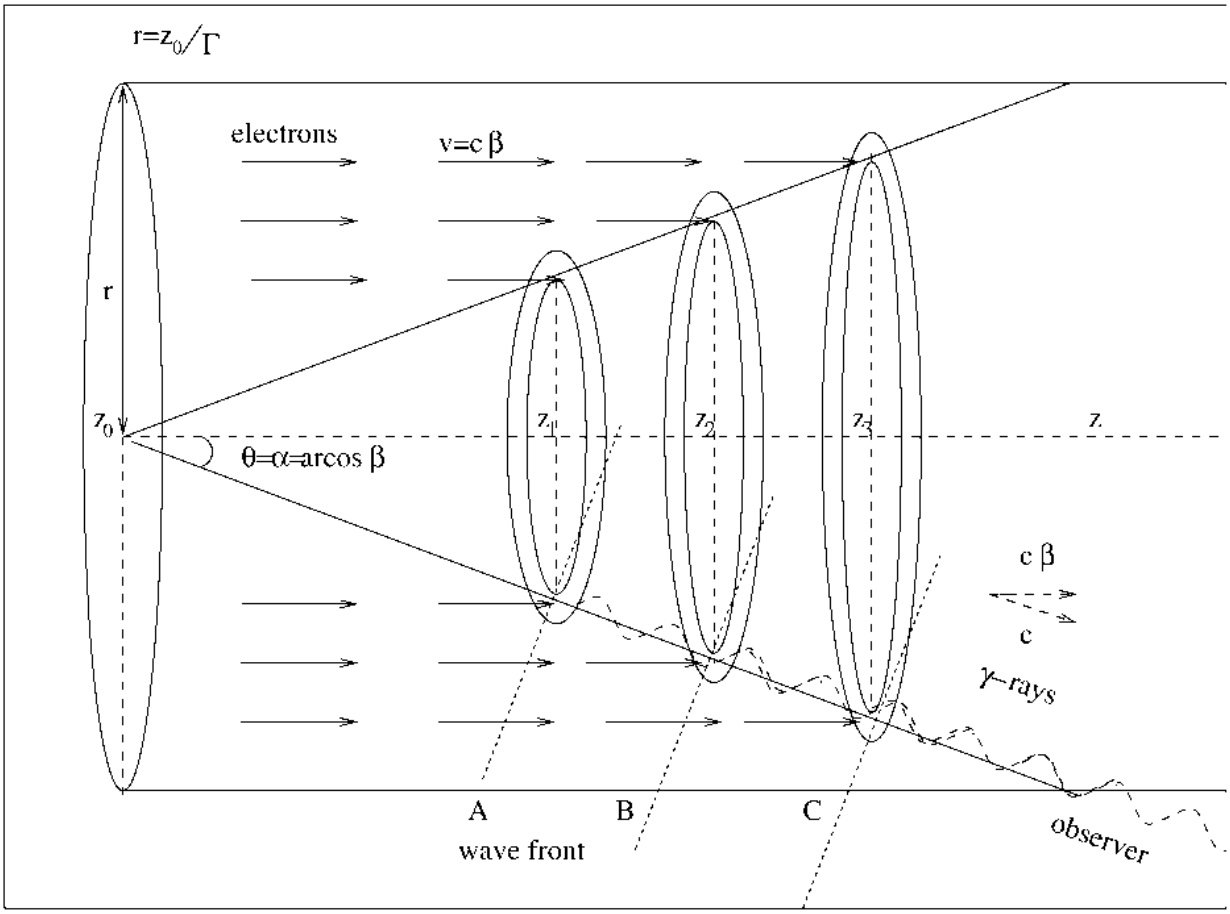

Figure 3: Model of the Jet of a Blazar from the observer's point of view [2].

where $s = z * \tan(\alpha)$, and α is the cone opening angle.

The z coordinate points down the axis of the jet

$$z = c\beta t \qquad (6)$$

With this geometry, the flux comes from a ring travelling down the cone.

$$F(t_{obs}) \propto \int_0^{\infty} \sqrt{(\frac{\partial x}{\partial t_{obs}})^2 + (\frac{\partial y}{\partial t_{obs}})^2}\,\partial t \qquad (7)$$

Due to the fact that the jet of a blazer is aimed almost directly at Earth, many of the particles in the jet exhibit superluminal motion. Superluminal motion occurs when an object appears to travel faster than the speed of light. This motion is accounted for both by the relativity factor and the $(1 - \beta\cos(\theta))$ part of Equation 4, the beaming factor. This equation is based on what we know about superluminal motion and how it is generally modeled by mathematics. Equation 4 defines the reference frame of the model as the observers reference frame. The observers frame is the frame in which superluminal motions is present. The relativity factor, or beaming factor is

needed to account for this motion, which does not occur in the particles rest frame. Equation 7 is very important because it describes the source flux as a function of observed time. Not only is it in the frame of the observer, but it is a description of the radiated energy from a source. Therefore it can be connected to our observations of Markarian 421.

There are a few key differences between the Salvati model and the Wagner model. The Wagner model assumes the blobs have a density that is low enough that they don't reabsorb emitted γ-rays, which results in generally broader flares than the Salvati model. The reason for this difference in curve shape is that denser blobs of particles in the relativistic jet generate flares with sharper, shorter rise and fall times. The Salvati model predicts that the blobs are dense enough to reabsorb emitted light for a given amount of time. This results in the diagram shown in Figure 3, where all of the shock fronts created by the injected blobs are only seen as rings by the observer. It is highly possible that both theories can be used to describe data that contains multiple or compounded flares in a single night. This would probably be the result of the Wagner theory describing the longer flares, and the Salvati model describing shorter flaring regions.

IV. VERITAS Telescope and Vegas Stages

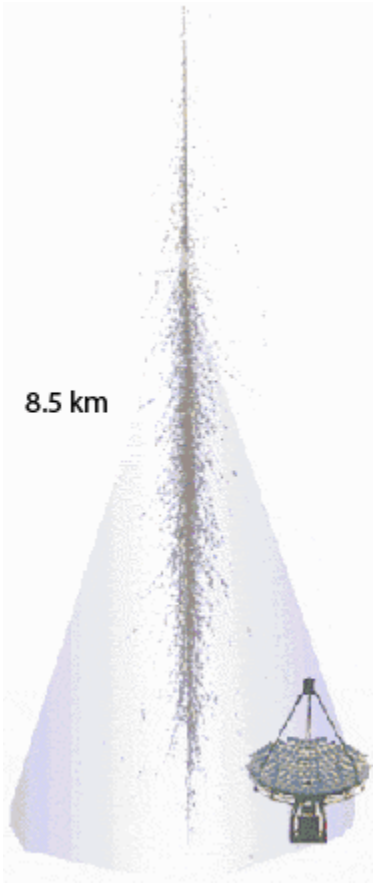

Figure 4: Virtual gamma ray air shower falling over the VERITAS telescope [6].

The Mrk 421 data light curve was generated by the Very Energetic Radiation Telescope Array System (VERITAS). VERITAS, as its name suggests, is a telescope array system that observes very high energy gamma radiation. The observed radiation falls within the range of 100 GeV to 50 TeV. The telescopes are located in Arizona at the Fred Lawrence Whipple Observatory base camp. Each one of the four telescopes in the array system is 12 meters in diameter. VERITAS was completed in January of 2007 and experienced first light that same year in April [5]. These telescopes rely on the imaging Cherenkov technique to make their observations. VERITAS is a ground based telescope that's main goal is to observe and analyze high energy astronomical sources. These sources emit high energy gamma rays in the TeV range. Gamma rays of this energy do not penetrate earth's atmosphere, which makes observing them from a ground based telescope very interesting.

Instead of observing the γ-radiation directly, VERITAS telescopes observe the chain reaction caused by high energy photons striking the top of Earth's atmosphere. When high energy gamma rays

$\gamma \rightarrow e^+ + e^-$ *production*
$e^+ \rightarrow e^+ + \gamma$ *radiation*
$e^- \rightarrow e^- + \gamma$ *radiation*
$e^+ + e^- \rightarrow \gamma$ *annhialation*

Table 1: Four possible electron, positron and photon interactions

collide with the atmosphere they interact with much lower energy protons and neutrons in the atmosphere which creates a "shower" of secondary particles. These secondary particles are all electrons, positrons, and more photons. Conservation of momentum causes the particles to move faster than the speed of light in air. These energized fast moving charged particles create Cherenkov radiation. Charged particles, such as electrons and positrons, are the only particles in the shower which emit Cherenkov light. Cherenkov radiation is a shock wave of electromagnetic radiation generated by the shower particles moving faster than the speed of light in air. In our case the particles energized by the gamma rays excite other particles because they are moving faster than the speed of light in the atmosphere. This phenomenon creates an air shower, which is detected and analyzed by the VERITAS telescopes when it eventually reaches the surface of our planet. Electromagnetic air showers are all electron-positron pair production, annihilation, and radiation. All of these particle interactions are described in Table 1.

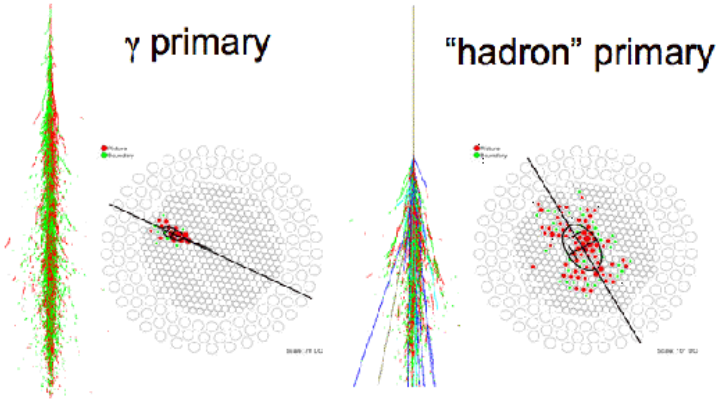

Figure 5: (Left) Pixel image of a gamma ray shower, (right) and pixel image of a hadron shower [6].

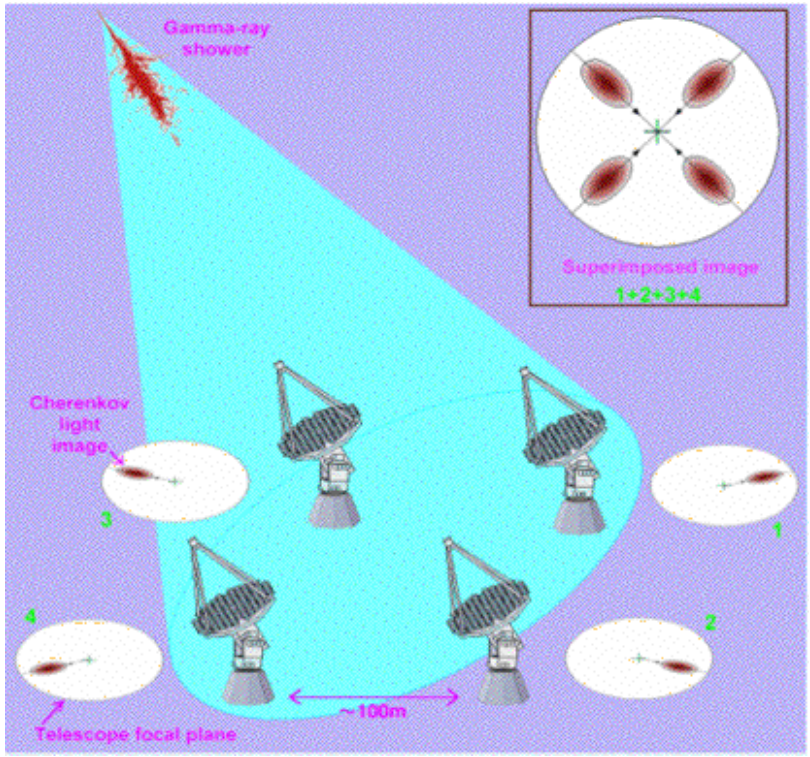

Figure 6: VERITAS Stereo imaging using all four telescopes in the array system [6].

Figure 4 shows an image of a gamma ray air shower falling in range of a VERITAS telescope. Air showers are generated by other materials like cosmic rays striking our atmosphere as well. In fact cosmic rays are a more frequent source of air showers than gamma rays. Cosmic ray air showers are a mix of all particles including $\pi^+, \pi^-, \pi^0, \mu^+, \mu^-$, etc. Figure 5 shows the observable difference between a gamma ray shower and a cosmic ray shower. Due to their frequent occurrence cosmic rays generate a considerable amount of background that must be discerned from the gamma ray showers by our gamma ray

telescope. This background appears in VERITAS data as background flux. Cosmic rays are subatomic particles in the atmosphere that have a high enough energy to be detected by VERITAS telescopes. The size and shape of an air shower is used to tell the difference between a cosmic ray or "hadron" shower and a gamma ray shower. This is one of the most necessary abilities of the VERITAS telescopes, because it improves the accuracy of the scientific results of the data. Stereo imaging allows shower images to be created that display the detection of the same air shower by all 4 VERITAS telescopes. Figure 6 shows an example of stereo imaging in action. Images of gamma ray showers will seem to point towards the center of the camera while cosmic ray showers do not. The use of multiple telescopes allows the VERITAS collaboration to detect smaller showers than they would be able to with the use of only one telescope. This is because the use of multiple telescopes allows air showers to be detected with a lower photon energy boundary coupled with higher energy resolution.

Figure 7: image of the 499 Photomultiplier tubes present at the focal point of each VERITAS telescope [6].

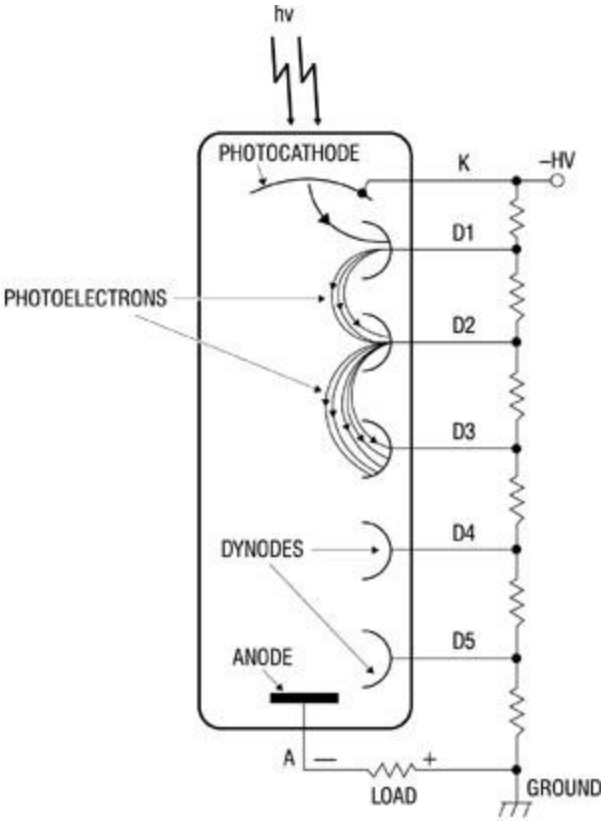

Figure 8: Circuit diagram of photomultiplier tube [7].

VERITAS is the second stage of a high energy astrophysics project at the Fred Lawrence Whipple observatory that started with the Whipple 10 meter telescope. Cherenkov light is ultimately detected by the VERITAS telescopes using an array of photomultiplier tubes (PMTs). Each telescope has 499 PMTs which detect incoming photons, as shown in Figure 7. This array of PMTs gives each telescope a pixel spacing of approximately 0.15 degrees. Each telescope also has a field of view (FOV) of 3.5 degrees [7]. A schematic of one of the PMTs used on the VERITAS telescopes is shown in Figure 8. Electronics then determine all of the needed information from incoming photons incident on the PMTs. Light is directed into the PMTs by approximately 345 hexagonal

mirrors that are coated to reflect the maximum amount of Cherenkov light.

The VERITAS telescopes count the incoming gamma rays, but not all of them. There are 3 different electronic trigger levels that help verify that VERITAS only detects a legitimate shower. The first of these trigger levels is the voltage discriminator level. This ensures that the VERITAS computers only count gamma rays that produce a voltage greater than the determined discriminator voltage when detected by the photomultiplier tube. The second electronic discriminator trigger is the fastbus crate. The fastbus crate makes sure that at least 3 neighboring PMTs are triggered in a given time window in order to identify the PMT trigger as a legitimate air shower detection. After passing through the first two discriminators, the shower data from all 4 telescopes is sent electronically to the main data hub via fiber optic cables. This main data hub runs the data through the third discriminator level. The third discriminator only accepts counts from triggered PMTs as a legitimate air shower if PMTs on 2 or more telescopes are triggered in a given time window.

Gamma rays detected by the VERITAS telescopes are organized and analyzed by our (VERITAS gamma Ray Analysis Suite) VEGAS software. This software analyzes each gamma ray in six different stages. VEGAS software is run using the C++ programming language. VEGAS stage 1 is the calibration stage. This stage determines the number of photoelectron counts per pixel in each of the PMTs. Stage 1 reduces the images using dark, flat, and bias images taken by the telescope. Stages 2 and 3 are currently integrated together as one stage of analysis. Stages 2 and 3 determine the biggest island of neighboring pixels. They also determine the Hillas parameters of the shower, the showers centriod x and y coordinates, length, width, and the sum of the photoelectron angles off of the black hole of the source. VEGAS stage 4 then combines the images from all of the telescopes to determine the parameters of the observed air shower. These parameters include the height and direction of the shower, as well as the energy of the initial gamma rays that caused the shower. The air shower is also reconstructed in this stage [8]. Discriminatory cuts are then made to the shower to select only the useable data from the observations. For our analysis we used the version 220 code release and the standard analysis cuts. Stage 6 is the final stage of VEGAS. This stage produces a final picture of the AGN by putting the recreated showers together. Stage 6 produces flux and light curve plots which can be studied and analyzed to learn about the physics of the AGN.

During the summer of 2010 I spent 3 weeks at VERITAS helping prepare the telescope for the observing season, which is all year except for the summer months when monsoons occur. In Arizona I swapped out worn telescope mirrors with clean ones freshly covered with reflective coating. After the mirrors were swapped out I took inventory on all of the mirrors on all 4 telescopes by climbing on them and recording their serial numbers. This allowed me to categorize the mirrors with their location on the telescopes and their most up to date information, which ultimately allowed me to report the length of time each mirror has been on the telescope and whether any mirrors need to be swapped out with freshly coated ones. I also assisted with the mirror alignment of the telescopes. Telescope alignment is done using a CCD camera and a bright star. The camera is placed at the focal plane of one of the telescopes. The star is then

brought into view of the telescope, and the intensity of its reflection in each mirror on the telescope is analyzed by the computer's raster Cam program. Manual adjustments are then made to the telescope mirrors in order to achieve optimal light reflection from the mirrors [9]. During my time in Arizona I also tested the reflectivity of the telescope mirrors. This is done by first placing a reflective target in front of the array of PMTs on the telescope, and attaching a CCD camera to one of the mirrors of the telescope. The reflective target is designed to reflect light incident upon it equally in all directions. The telescope is then used to locate a star. It is important that the star selected is not too bright or observed for too long otherwise it might saturate the CCD camera. The reflectivity measurement will not be accurate if the CCD becomes saturated. The reflectivity measurement compares the brightness of the observed star with the brightness of its reflection from the target. From this data the average reflectivity of the telescope mirrors can be determined.

V. Markarian 421 Observations

Markarian (Mrk) 421 is the brightest observed blazer in the night sky. It has an observed apparent magnitude of about 13. This is pretty bright considering it has been determined to be about 400 million light years away. This distance from Earth is so vast that it actually effects the light traveling to Earth from the blazer. Mrk 421 has a red shift of z=0.031. This is expected because gamma rays such as those emitted by Markarian 421 will be absorbed by the intergalactic infrared background if the source has a red shift greater than or equal to 0.5 [4]. This blazar sits at a Right Ascension and Declination of 11hr 04 min 27 sec and 38deg 12min 31sec respectively. It can be observed in the night sky, with a telescope under the right conditions, by looking linearly away from the two brightest stars (or pointer stars) in the big dipper in the direction of the brightest star in the constellation. The small red shift and intense brightness of the source are two reasons why it was the first blazar detected at TeV energies, or energies above 500 GeV [2]. Markarian 421 is an interesting source because it has a history of flaring, but that's not all. The timing, duration, and rise and fall time of these flares are asymmetric, which means that the flare rises over a different amount of time than it falls back to its steady state. Both the long and short term flare timing does not appear to follow any periodic pattern. This suggests that the cause of these flares is something other than the periodic rotation and precession of the Blazar. This paper focuses on the cause of only the short term flares, though they may be related to the cause of the long term flares. As mentioned before, the short term flares are believed to be caused by the injection of blobs of relativistic electrons into the jet.

Data from this flare can be found in the VERITAS data store. The goal of this paper is to use the VERITAS observations of Markarian 421 to generate a light curve of the source in its flaring state, and to fit a theoretical model to this data.

The May 3rd 2008 flare was not chosen because the flare was short. After looking through the Markarian 421 data the 2008 flare was found to be the most complete flare with very clear visible evidence of short term rapid flaring as described in the previously mentioned Markarian 421 theory papers. This is important because Markarian 421 can only be observed at night.

Date (m/d/y)	Run	Source	UTC	Duration (min.)	Sky	Elevation	Azimuth	Frequency (Hz)
5/3/2008	40672	Mrk421	04:10	20	A	80	313	224
5/3/2008	40673	Mrk421	04:33	20	A	76	301	224
5/3/2008	40674	Mrk421	04:54	20	A	72	300	221
5/3/2008	40675	Mrk421	05:15	20	A	69	296	218
5/3/2008	40676	Mrk421	05:36	20	A	63	294	210
5/3/2008	40678	Mrk421	06:01	20	A	59	295	205
5/3/2008	40679	Mrk421	06:22	20	A	55	293	198
5/3/2008	40680	Mrk421	06:43	20	A	51	294	191
5/3/2008	40681	Mrk421	07:04	20	A	47	296	179
5/3/2008	40682	Mrk421	07:26	20	A	42	295	168
5/3/2008	40683	Mrk421	07:48	20	A	38	297	153
5/3/2008	40684	Mrk421	08:09	20	A	34	298	142

Table 2: Markarian 421 May 3, 2008 Flare Observation Run List

Therefore VERITAS can observe this source for no more than 8 or 9 hours continuously. This constraint prohibits the telescope array system capturing gamma rays for an entire long term flare, but it is still enough continuous observing time to capture data for full continuous short term flares. The VERITAS database has to be very organized because when the only information one has to analyze is light, every categorization of the photons is important. The light curve is ultimately generated by running the high energy photon data from Markarian 421 observations through the 6 stages of VEGAS. The chosen data was further reduced by selection due to its quality. The quality of each run is given a grade A-F based on the weather on the night of observation. Our light curve was generated using only observations with "A" weather conditions. The run list, or list of runs chosen to generate the spectrum and light curve used for this analysis is shown in Table 2.

VI. Light Curve Analysis

Figure 9 shows the light curve data of the 2008 flare of Markarian 421 generated by VERITAS. Upon close inspection of Figure 9 one can see that Markarian 421 seems to have a normal state flux of about $2 \times 10^{-6}\gamma - \text{ray}/(\text{m}^2\text{s})$. The lightcurve exhibits a long term flare about 3.4 hours in length and about $4 \times 10^{-6}\gamma - \text{ray}/(\text{m}^2\text{s})$ in amplitude above the steady state flux of the source.

Once the light curve for the flare in question has been generated we move on to our main goal, fitting the theoretical model to the data. To properly fit the theory to the data we first attempt to fit the simplest, most general theory. This helps prevent us from overlooking any possibilities. The degree to which an attempted model fits the actual data is determined by conducting a chi-squared test. The chi-squared test is a test to determine whether observations or data are consistent with a theoretical distribution [10]. This test is done by overlaying the data

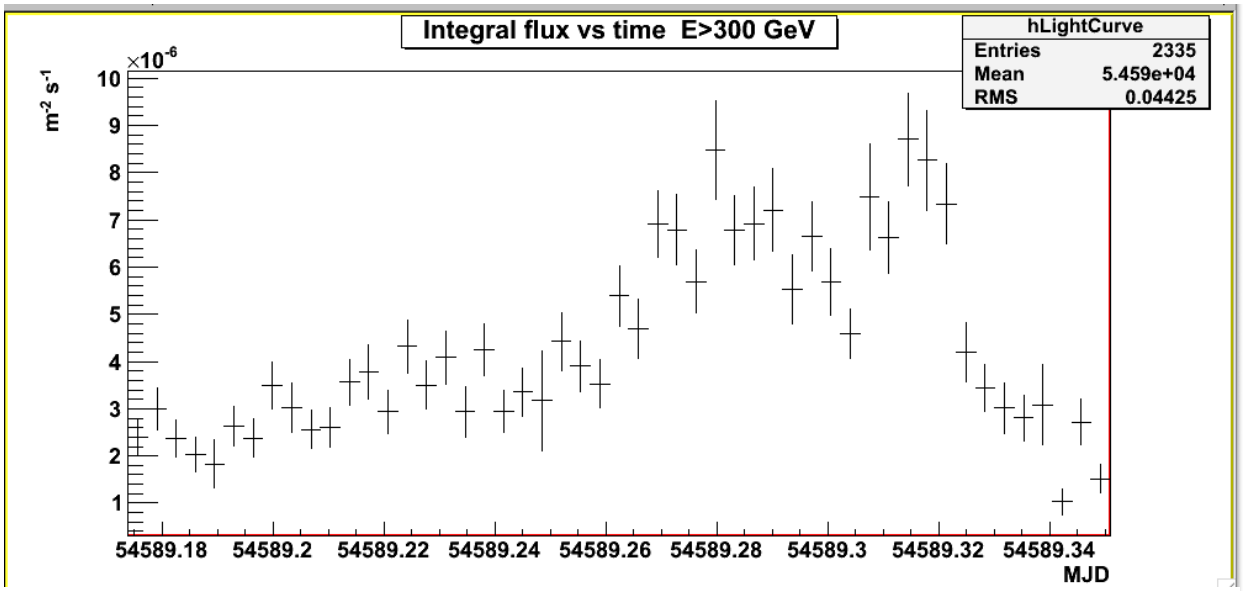

Figure 9: Light Curve of the Blazar Markarian 421. This Light Curve was observed over a duration of 8 hours on the night of May 3rd 2008. The y-axis is the amount of flux entering the detection area every second. The x-axis is the date of the flare in units of Modified Julian Date (MJD).

points with the theory curve and comparing their flux values at each time increment or x-axis value. This paper uses the reduced chi-squared (χ^2) value, defined by

$$\chi^2 = \frac{1}{d}\sum_{k=1}^{n}\frac{(O-E)^2}{E} \qquad (8)$$

to determine the consistency of any given theoretical model that has been overlaid with the data. The d variable in equation 8 describes the number of degrees of freedom, $d = n - c$, where n is the number of bins that the data is organized in and c is the number of constraints or adjustable parameters. The O variable is the observed value in any given bin, and the E variable is the expected value in the same bin. In our case, the observed values are our data points, the expected values are our theory curves, and the bins are time increments. A result of $\chi^2 \gg 1$ means that the expected values do not agree with the observed values, in other words the theory does not fit the data. The theory and data values are proven

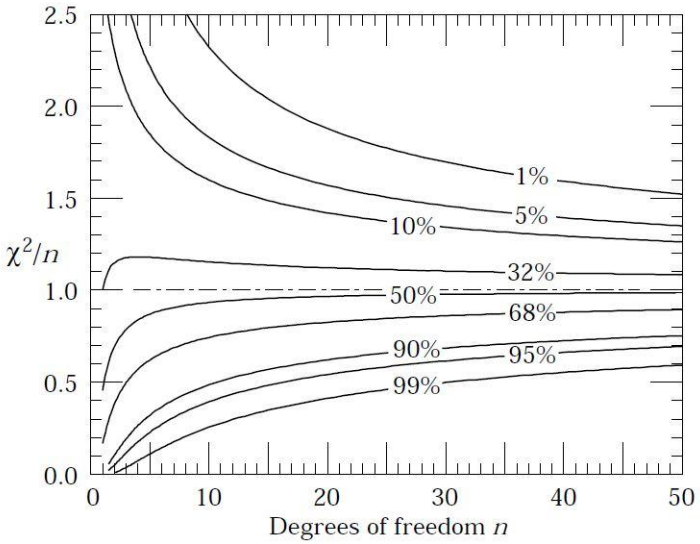

Figure 10: A plot of reduced chi-squared values vs. degrees of freedom. The solid lines indicated the probability/p-value of the regions of the plot.

to be in satisfactory agreement if $\chi^2 \lesssim 1$ [10]. The amount of agreement that a theoretical model has with the data is described by the probability or "p-value" of a χ^2 test. The probability is based on the chi squared value and the number of degrees of freedom associated with the fitted curve, as shown in Figure 10. A probability greater than 10% shows a satisfactory amount of agreement between data and theory [11].

The first attempt to model the data, Figure 11, was done using a linear model, which returned a χ^2 value of 7.75. The probability of this value was much less than 10%. The fact that the linear fit is not consistent with the data is important because it proves that there is actually a flare in the light curve. It is important to note that the last 3 data points, those occurring at the latest time, are not used when generating χ^2 values. The reason for this is that 2 out of 3 of those points are below the steady state value of the blazar. Therefore they are considered to be innacrate data measurements, porbably caused by a fault in the PMT that made the observation.

For the next attempt, a model consisting of a single flare generated using the Wagner model (Equation 1) was fit to the data. This theoretical model overlaying the data is shown in Figure 12, along with its χ^2 value in the upper left corner of the plot. A reduced χ^2 value of 2.87 is much larger than 1, due to its lower than 1% probability, and therefore not a good fit to the data. The reason that one Wagner curve does not fit this flare is because the flare appears to have two flaring regions where the flux from the source is at a peak. Each of these flares is about 1.5 hours in length and increases the flux of the long term flare by about $2 \times 10^{-6}\gamma - \text{ray}/(\text{m}^2\text{s})$. Figure 12 demonstrates the best possible determined fit to the data, and it is clearly evident that the data cannot be fit by this model.

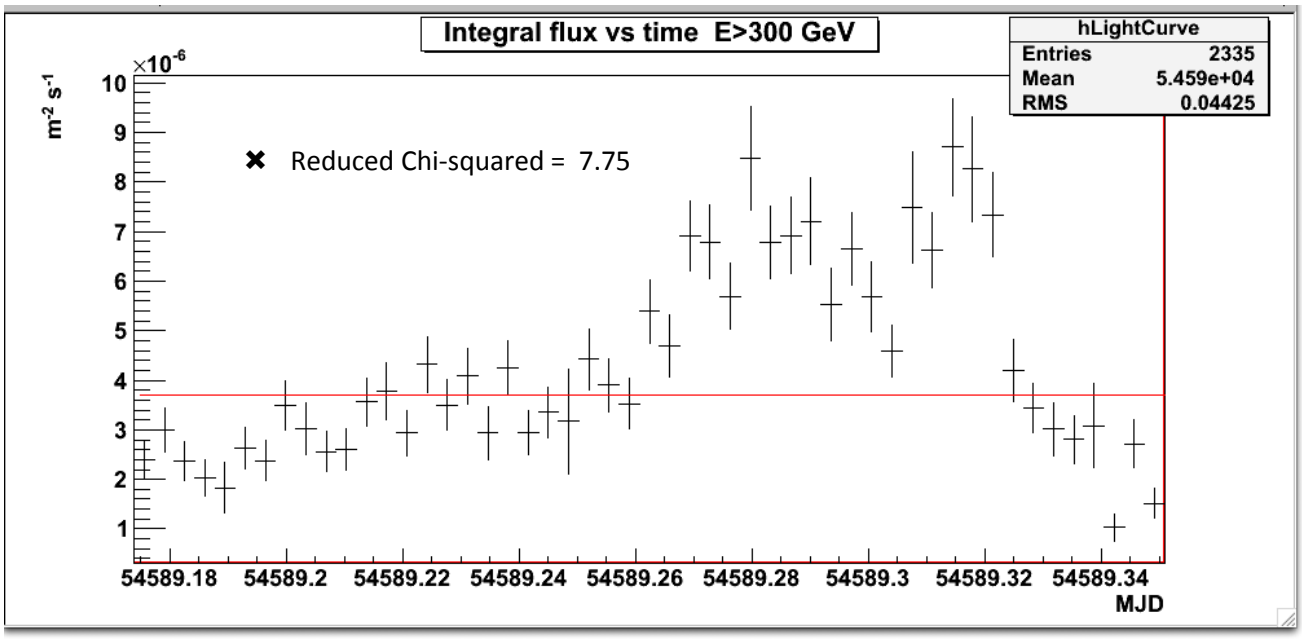

Figure 11: Light Curve of Mrk 421 with linear fit. The chi-squared value is shown in the upper left corner.

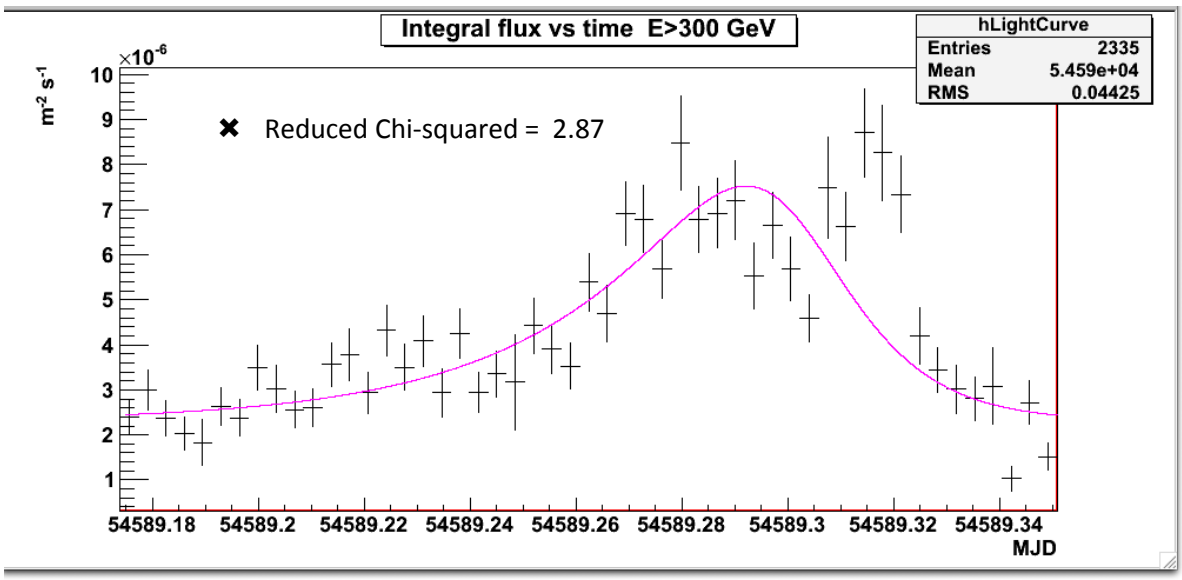

Figure 12: Light Curve of Mrk 421 fit with single Wagner theory curve. The chi-squared value is shown in the upper left corner.

After the last attempt it was evident that we needed to get a little bit fancier with our model. The next attempt, shown in Figure 13, is a compilation of three Wagner theory curves interpolated on top of one another. The parameters of each curve have been adjusted to fit the appropriate flaring region. This curve does a better job of fitting all flaring regions individually including the dip in between the two most prominent regions. The χ^2 value is 1.26, with a probability of greater than 10%. This shows a significant amount of agreement between the theory and the data.

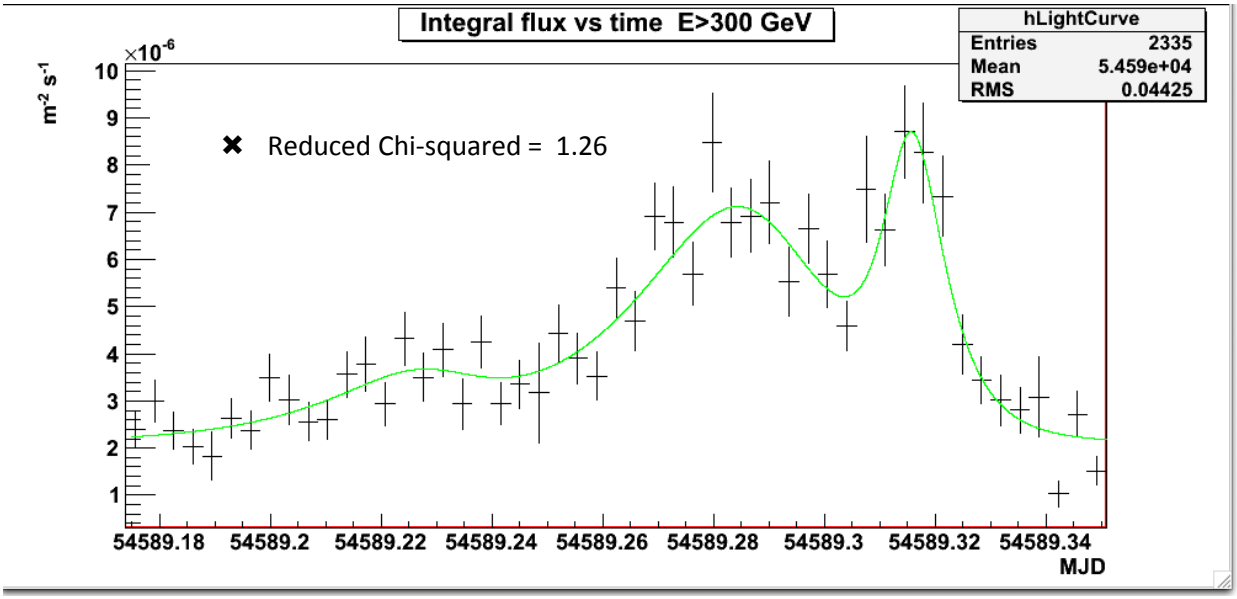

Figure 13: Light Curve of Mrk 421 fit with triple Wagner theory curve. The chi-squared value is shown in the upper left corner.

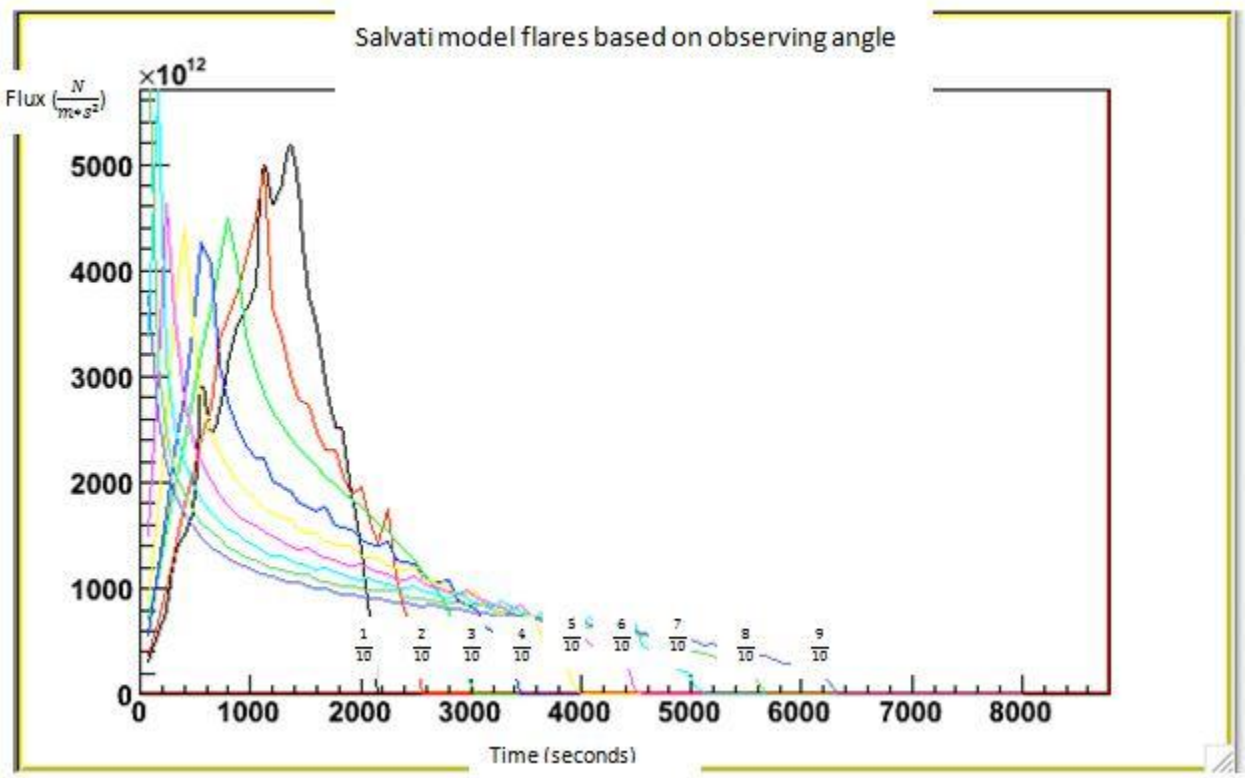

Figure 14: Theoretical light curves generated by the Salvati model. The fraction of the jet opening angle that causes each flare is posted on top of it respective colored curve.

The next model consists of two curves generated by the Salvati model. The Salvati model is generally used to fit sharper curves than the Wagner model. At the same time it is less malleable than the Wagner model because its parameters are more rigid and allow for less adjustment of the actual shape of the flare. The Salvati model is based on the observers point of view. The main parameter that defines the shape of the generated flare, such as its amplitude and width, is the angle of the relativistic blazar jet in the reference frame of the observer. An observer on Earth can only observe down the jet of Mrk 421 at one angle at a time. Therefore even a theoretical model that uses multiple Salvati model flares can only accurately generate flares with rougly the same amplitude and width. An array of Salvati model flares is shown in Figure 14. Each flare is generated using a different observing angle and is identified by a different color. We attempted to fit two Salvati curves interpolated on top of one another to the 2008 light curve data of Mrk 421. The observing angle that proved most agreeable with the data was one-tenth of of the optimal jet viewing angle. The optimal jet viewing angle of Mrk 421 is 0.1 radians or 5.8 degrees, so one-tenth of that value would be 0.01 radians, or 0.57°. The fit gave a χ^2 value of 3.81, with a probability of much less than 5%, indicating that the model did not fit the data. The model is shown in Figure 15. The resulting reduced χ^2 only compares the theory curve to the data points of the main flaring region. More specifically, the first 21 light curve data points and the theory curve in those corresponding time bins are not used to calculate

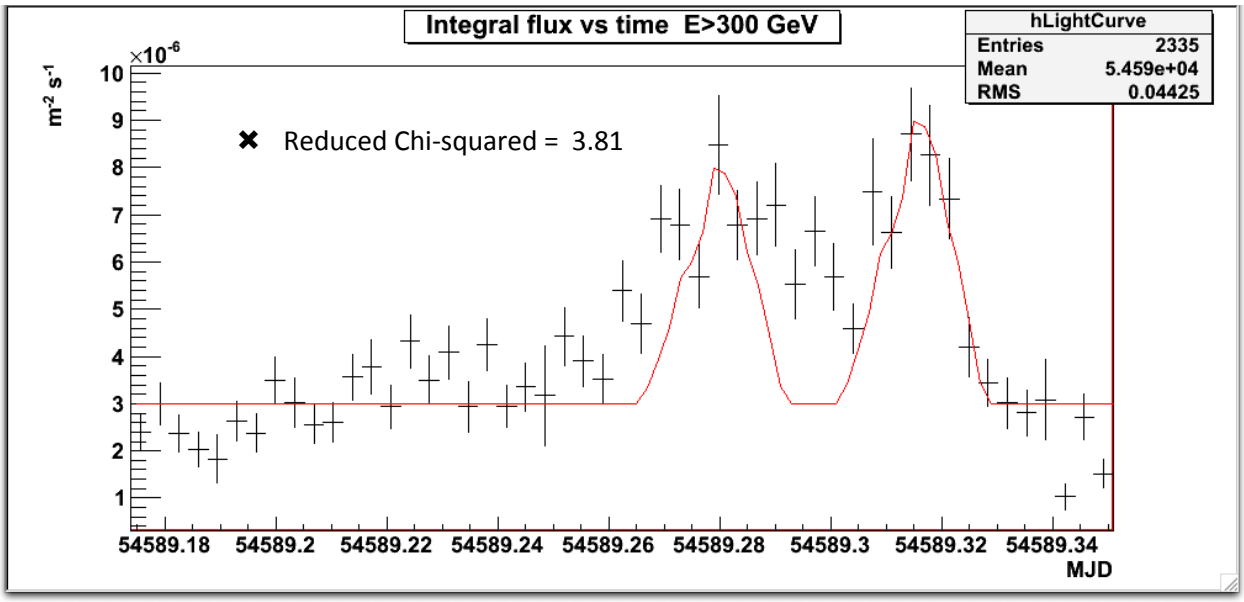

Figure 15: Light Curve of Mrk 421 fit with double Salvati theory curve. The chi-squared value is shown in the upper left corner.

this χ^2 value. This is because Figure 15 is an attempt to fit the light curve using only Salvati curves, which are never broad enough to fit the smallest flaring region early in the light curve. A straight line was fit to this part of the curve, and was not used as part of the χ^2 test because it was already determined that a straight line does not fit the data. The reason for the lack of agreement is that the flaring regions in the data do not have the same width. The first flaring region appears to be broader than the second. Therefore this data cannot be fit purely by multiple Salvati curves which can only be modeled with one oberving angle.

Another model was made using a combination of both the Wagner and Salvati models to

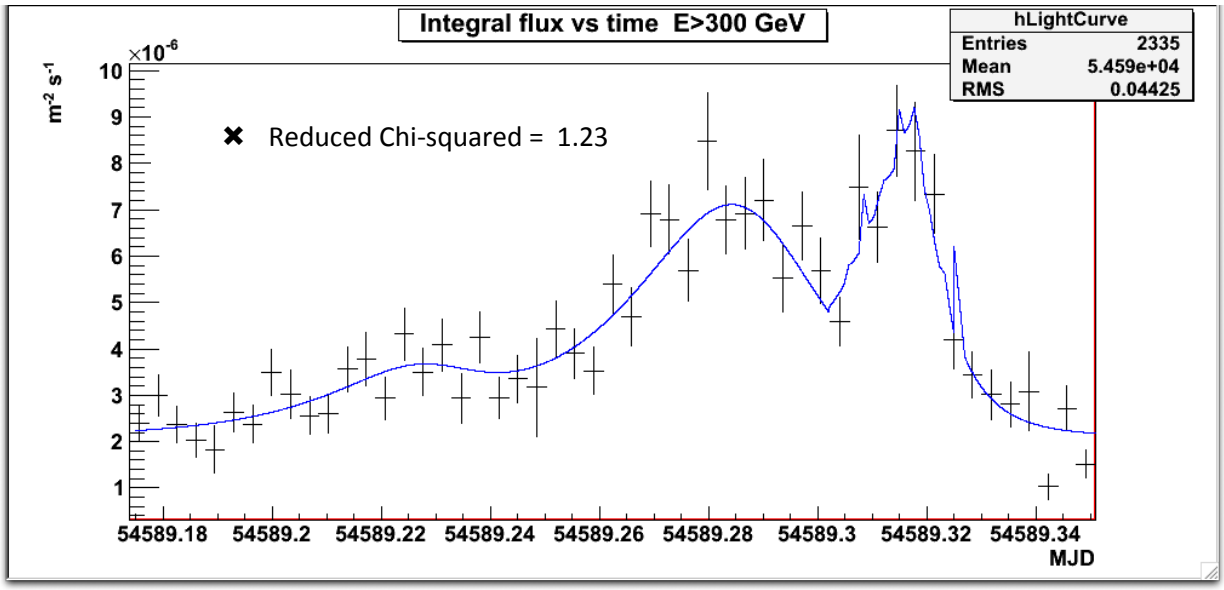

Figure 16: Light Curve of Mrk 421 fit with combination Wagner/Salvati theory curve. The chi-squared value is shown in the upper left corner.

generate a theory light curve. The Wagner model was used to fit the broader flaring region and the Salvati model was used to fit the sharper region. This produced a χ^2 value of 1.23, with a probability of greater than 10%. Therefore, this model shows significant agreement with the data. The combination model fit is shown in figure 16. The Wagner model states that smaller rise and fall flare times indicated that high energy gamma rays were emitted from a blob in the jet closer to the jet origin. The Salvati model theorizes that the blobs are denser than those theorized in the Wagner model. This is very interesting because of the order of the flares in the data. The sharper flaring region which is also fit by a smaller rise and fall time occurs after the broader flaring region. This suggests that at least the last two flaring regions of this flare were caused by two separate blobs in the jet, rather than one blob with multiple emissions. If the flaring regions were caused by one blob the sharper flaring region would be expected to appear before the broader one. These results suggest that one blob emitted high energy photons from the blazar jet and then another, denser blob emitted high energy photons from a smaller region of the jet closer to the central super massive black hole. The first, smallest, flaring region is fit with a sharper theory curve than the second flaring region. Therefore there is not enough evidence to suggest that the first and second flares were caused by emissions from the same blob or two separate blobs.

Using Equations 2 and 3 we were able to calculate the upper limit of the radius of the region of the jet from which the high energy photons were emitted. The calculation begins with Equation 2, whose variables are known from [2]. For Mrk 421, $\Gamma = 10$, z=0.031, $\beta = 0.995$, and $\theta = 0.1$. These numbers are plugged into equation 2 to find the Doppler boosting factor δ. I found that in this case $\delta = 9.7$. Then I put the δ value in Equation 3 and multiply it with the flare rise time of each flaring region. The rise times of the three flaring regions present in the data are, in chronological order, $\tau_{rise} = 0.3$ hours, $\tau_{rise} = 0.32$ hours, and $\tau_{rise} = 0.07$ hours. The first smallest flare was calculated to be emitted from a region of the jet with a radius of $R < 6286$ million km . Table 3 indicates that the size of this emission region is roughly equivalent to a distance from our Sun that is slightly larger than the average distance of Pluto. The middle flare was calculated to be emitted from a region of the jet with a radius of $R < 6705$ million km . Table 3 indicates that the size of this emission region is roughly equivalent to a distance from our Sun that is about 80 million km larger than the average distance of Pluto. The final and sharpest flare was calculated to be emitted from a region of the jet with a radius of $R < 1467$ million km. Table 3 indicates that this emission region is equivalent in size to a distance from our sun that sits in between the average distances of Saturn and Uranus, but is only slightly larger than that of

Planet	Distance from Sun
Saturn	1428 million km
Uranus	2974 million km
Neptune	4506 million km
Pluto	5913 million km

Table 3: Average distance from the sun of planets in our solar system

Saturn. The size of the emission regions are rather small compared to the overall size of the blazar. The blazar is equal to or larger than the size of many galaxies, but the emission regions have radii that are the size of solar system distances. This is unexpected because galaxies are vastly larger than the solar systems they contain. Therefore one would not immediately expect to find solar system sized observable parameters on a galactic sized object. In comparison, the central super massive black hole near the origin of the particle jet in Mrk 421 has a Schwarzschild radius of R = 295 million km [4]. The radius of the black hole is calculated with

$$R_S = \frac{2GM}{c^2} \qquad (9)$$

where G is the universal gravitation constant, c is the speed of light in a vacuum, and M is the mass of the black hole. The super massive black hole in the center of Mrk 421 has a mass 100 million times that of our sun, or 10^8 solar masses [4]. The upper limits of the first second and third flare (in time) emission region radii are approximately 21, 23, and 5 times larger than the Schwarzschild radius of the black hole respectively. This indicates that the third flare occurred relatively close to the central super massive black hole, and therefore also the jet origin.

VII. Conclusion

The results of the analysis show that the Wagner model, which is able to fit broader flares than the Salvati model, is a better theory for fitting the first two flaring regions in the time sequence of the data light curve. The Wagner model proves to be in agreement with all 3 flaring regions of the data light curve, because the theory curves created using this model produce a χ^2 value of $\chi^2 = 1.26$ when overlaid with the data. This is very close to 1 as indicated by its greater than 10% probability. The results also indicate that the Salvati model can also be used to accurately fit the final flaring region of the data light curve. In Figure 16 the first two flaring regions were fit with Wagner model curves and interpolated with a Salvati curve to fit the final flaring region. This produced a χ^2 value of $\chi^2 = 1.23$ indicating substantial agreement with the data.

The fact that the last two flaring regions occur chronologically starting with the broadest flaring region and ending with the sharpest indicates that each of the flares was caused by a separate blob present in the jet. This is important because it provides a useful insight to the specific jet constitution needed to generate a light curve like the May 2008 flare.

The rise and fall times used to create the best fitting Wagner model theory curves were analyzed further to determine the size of the blazar jet emission region from which the high energy gamma rays that created the light curve flares were emitted. The region sizes of the earliest, middle, and latest flaring regions were found to be $R < 6286$ million km, $R < 6705$ million km, and $R < 1467$ million km respectively. These resulting region sizes agree with [4], and conclude that emission regions the size of planetary solar orbits in our solar system

are found on galactic sized objects such as a blazar. This is a very unexpected and interesting result. The smallest emission region is only about 5 times larger than the radius of the central super massive black hole, indicating that the observed gamma rays were emitted very near the origin of the jet.

To ensure the accuracy of the experiment we had to make sure that the data was of good quality and sufficiently free of backgrounds. It was also important that the right number of constraints were used when calculating the χ^2, otherwise the theory would have appeared to be more or less in agreement with the data than it actually was.

For this the most up to date discriminatory data cuts were used. In the future perhaps there will be data cuts that provide even better quality and more accurate data. It would be interesting to see if the theory parameters changed at all with updated cuts.

VIII. Acknowledgements

This project is supported by the National Science Foundation (NSF), the Cal Poly Physics Department, and the Cal Poly College of Science and Mathematics. I would like to thank Dr. Jodi Christiansen for advising me on this project and proofreading my final report.

IX. References

[1] Wagner R. M., Schwiezer T., & Lorenz E. 2009 *A Statistical Study of Sub-Hour Flares of the VHE Gamma-Ray Emission of Markarian 421 During a High Flux State in 2001*. ICRC.

[2] Salvati M., Spada M., &Pacini F. 1998 *Rapid Variability of Gamma-Ray Blazars: A Model for Markarian 421*. The Astrophysical Journal.

[3] http://www.mpifr-bonn.mpg.de/div/vlbi/ckp08/images/AGN/jet.gif

[4] Fegan, David J. 1998 *TeV Variability and Flaring of the Blazar Markarian 421*. Nuclear Physics B.

[5] http://veritas.sao.arizona.edu/wiki/index.php/Main_Page

[6] http://veritas.adlerplanetarium.org/project/

[7] http://veritas.sao.arizona.edu/content/view/215/87/#ACT%20Technique

[8] http://veritas.sao.arizona.edu/OAWGwiki/index.php/Overview

[9] http://veritas.sao.arizona.edu/wiki/index.php/Mirror_Alignment

[10] Taylor, John R. *Error Analysis: The Study of Uncertainties in Physical Measurements.* Sausalito: University Science Books, 1997

[11] http://www-pdg.lbl.gov/2010/reviews/rpp2010-rev-statistics.pdf